AIAA JOURNAL
Vol. 54, No. 10, October 2016

Technical Notes

TECHNICAL NOTES are short manuscripts describing new developments or important results of a preliminary nature. These Notes should not exceed 2500 words (where a figure or table counts as 200 words). Following informal review by the Editors, they may be published within a few months of the date of receipt. Style requirements are the same as for regular contributions (see inside back cover).

Development and Validation of a Grid-Free Viscous Solver

K. Anandhanarayanan,* R. Krishnamurthy,*
and Debasis Chakraborty*
Defence Research and Development Laboratory, Hyderabad 500 058, India

DOI: 10.2514/1.J054863

I. Introduction

NUMERICAL simulation of the flowfield of a practical configuration poses severe difficulty due to complex grid-generation procedures. A Cartesian grid with near-wall extruded grids [1], chimera or overset grids [2], grid-free methods [3], and a combination of the aforementioned methods [4] is used to solve flow past complex configurations. The grid-free methods operate on a distribution of points in the domain and require a set of supporting nodes around each point to evaluate the spatial derivatives of the governing fluid equations. The point distribution can be obtained from structured, unstructured, Cartesian, hybrid, or overlapped meshes, or a random distribution of points. In recent years, quite a few grid-free methods were proposed in the field of compressible fluid flow. Among them, the least-squares kinetic upwind method developed by Deshpande et al. [5] has received much attention of researchers and been applied to number of complex flight vehicle configurations. Recently, the method was successfully applied to a store separation dynamics problem using a chimera cloud of points [6]. Batina [7] developed a gridless method that used the least-squares method with the unbiased support of points for the discretization of spatial derivatives. Artificial viscosity is used to stabilize the solutions and applied to inviscid and laminar flows. Lohner et al. [8] developed a finite point method, in which an upwind scheme was used to stabilize the solutions, and applied it to inviscid compressible flows. In the finite point method, the direction of upwinding is based on coefficients of the least-squares discretization, which is purely geometric. In recent years, the grid-free method has been successfully applied to simulate turbulent flow past complex flight vehicle configurations [9,10]. These methods used either overset grids or extruded layers of points near the wall, along with Cartesian grids in the offbody region, to get the distribution of points; and neighbors are obtained using search algorithms guided by grid information, which is therefore known as the semimeshless method. Lohner et al. [8] developed the advancing point generation method to generate a cloud of points, and the neighbors of those points were obtained using a local Delaunay triangulation. The applications, so far, are limited to subsonic and transonic flows. In the present work, a grid-free Euler and Navier–Stokes (GEANS) solver has been developed using a gridless method [7] with upwind fluxes for flow stabilization, and it has been validated for hypersonic flows at higher angles of attack. One of the main drawbacks of the grid-free methods is the lack of conservation. Katz and Jameson [11] enforced conservation by modifying weights in the least-squares discretization. However, such modified weights may become negative for certain distribution of points that leads to nonpositive solutions. Chiu et al. [12] proposed a method of generating meshless coefficients with conservation constraints at the discrete level; however, this method was complex to implement for three-dimensional (3-D) problems with an anisotropic distribution of points. In the present work, high-speed flows are simulated without enforcing the conservation property. A detail experimental results [13] for an all-body hypersonic aircraft is available for comparison of aerodynamic forces and moments in addition to local flowfields. The flowfield around the geometry is very complex, which involves strong compressions in the windward side and strong expansions in the leeward side, with flow separation and vortices at a hypersonic Mach number. Furthermore, high-aspect-ratio grid cells are required to resolve the very fine details of the flowfield. The simulation of such flowfields requires a robust flow solver that can handle both strong oblique shock wave and high expansion regions, as well as be accurate enough to resolve the boundary layer. Therefore, the aforementioned configuration is considered for validating the grid-free Euler and Navier–Stokes solver [14] at hypersonic speed and the results are compared with the experimental values. The geometry considered for validations in the present work is simpler and amenable for generation of simple structured grids. Therefore, structured grids are generated around the body to get a distribution of points and supporting nodes are obtained using the structured grid adjacency relation.

II. Three-Dimensional Navier–Stokes Equations

The three-dimensional compressible full Navier–Stokes equations can be written in Cartesian coordinate systems as

$$\frac{\partial U}{\partial t}+\frac{\partial F^j}{\partial x_j}=\frac{\partial G^j}{\partial x_j} \tag{1}$$

where t denotes time. The state and flux vectors are defined as

$$U=\begin{pmatrix}\rho\\ \rho v_i\\ \rho e\end{pmatrix}\quad F^j=\begin{pmatrix}\rho v_j\\ \rho v_i v_j+p\delta_{ij}\\ v_j(\rho e+p)\end{pmatrix}\quad G^j=\begin{pmatrix}0\\ \tau_{ij}\\ v_l\tau_{lj}-q_j\end{pmatrix} \tag{2}$$

where ρ is density; v_i are the velocity components corresponding to Cartesian coordinates x_i; e is the total energy per unit mass; p is pressure; τ_{ij} is viscous stress; and q_j is the heat flux. The turbulent viscosity μ_T is determined using the Spalart–Allmaras one-equation turbulence model [15].

The governing equations for compressible fluid flow consist of spatial and temporal partial derivatives. The main difference among various methods like finite volume, finite difference, finite element, and grid free is the discretization of spatial derivatives. In the grid-free method, the derivatives of fluxes at a point are discretized using the

Received 5 November 2015; revision received 20 April 2016; accepted for publication 24 April 2016; published online 4 July 2016.

*Scientist.

fluxes at its supporting nodes. Consider a domain Ω of R^3 (Fig. 1). The spatial derivatives of fluxes at point i are approximated as a function of fluxes at its n neighbors in the cloud $C(i)$. The discretized spatial derivatives at point i can be written as

$$\frac{\partial F^1}{\partial x_1} + \frac{\partial F^2}{\partial x_2} + \frac{\partial F^3}{\partial x_3} = \sum \tilde{a}_{ik} F^1_{ik} + \sum \tilde{b}_{ik} F^2_{ik} + \sum \tilde{c}_{ik} F^3_{ik} \quad (3)$$

The coefficients a_{ik}, b_{ik}, and c_{ik} for edge ik are evaluated using a weighted least-squares method as

$$\begin{Bmatrix} \tilde{a}_{ik} \\ \tilde{b}_{ik} \\ \tilde{c}_{ik} \\ \tilde{d}_{ik} \end{Bmatrix} = [A^T A]^{-1} \begin{Bmatrix} w_{ik} x_{1ik} \\ w_{ik} x_{2ik} \\ w_{ik} x_{3ik} \\ w_{ik} \end{Bmatrix} \quad (4)$$

where

$$A = \begin{bmatrix} w_{i1}x_{1i1} & w_{i1}x_{2i1} & w_{i1}x_{3i1} & w_{i1} \\ w_{i2}x_{1i2} & w_{i2}x_{2i2} & w_{i2}x_{3i2} & w_{i2} \\ \cdots & \cdots & \cdots & \cdots \\ w_{in}x_{1in} & w_{i1}x_{2in} & w_{i1}x_{3in} & w_{in} \end{bmatrix},$$

$$x_{jik} = (x_{jk} - x_{ji}) \quad \text{and} \quad w_{ik} = 1/\sqrt{\sum_{j=1}^{3} x^2_{jik}}$$

The preceding discretization using fluxes at neighboring points is like central differencing; hence, it is inherently unstable. Therefore, the upwind fluxes are evaluated at the midpoint of the edge ik (shown as a star in Fig. 1). The left and right fluxes are evaluated using a modified Roe scheme [16] with variables at point i and the neighboring point k, respectively. Then, the aforementioned spatial discretization procedure is applied using the fluxes at midpoints to evaluate the spatial derivatives of the inviscid fluxes. This discretization procedure leads to solutions that are first-order accurate in space, and they are not sufficient for practical applications. The second order of accuracy is obtained by extrapolating the primitive variables to the midpoint using primitive variables and their derivatives at points i and k to evaluate the left and right upwind fluxes, respectively. The Barth's MIN-MAX limiter [17] is used to ensure monotonicity in the solution. The viscous fluxes are evaluated at the midpoints using the average of the left and right variables and their derivatives; then, similar to inviscid fluxes, the viscous fluxes are discretized. The spatial derivatives of primitive variables required for evaluation of second-order-accurate inviscid fluxes and stress terms in viscous fluxes are also obtained using the least-squares method with variables at points i and k. The temporal term is approximated using a first-order forward difference, and the discretized governing equations are solved using the lower–upper symmetric Gauss–Seidel method. The one-equation Spalart–Allmaras turbulence model is used for closure, and the spatial derivatives of the turbulent variable are obtained to be similar to the mean flow equations.

III. Validation of the Code

A code has been developed using the aforementioned formulation and is referred to as the grid-free Euler and Navier–Stokes solver. The GEANS solver is validated for turbulent flow past a hypersonic all-body configuration.

The hypersonic all-body configuration is a double-wedge body configuration with elliptical cross sections, as shown in Fig. 2. The body has a delta planform with 75 deg sweptback leading edges. The forebody is an elliptic cone, and the afterbody has elliptical cross sections. The maximum cross-sectional area of the body is located at the junction of the forebody and the afterbody, which is at two-thirds of the body length from the nose. The reference area is the planform area, the reference length is the body length, and the moment center is at 0.55 of the length of the body from the nose. Two structured algebraic grids are generated with a size of 0.2 and 1.3 million points for the grid-dependent study. The turbulent flow simulations are carried out using the GEANS code at a freestream Mach number of 7.4 and angles of attack of 0, 5, 10, and 15 deg. The Reynolds number is 15×10^6, based on the length of the geometry. An isothermal wall boundary condition is applied on the surface with a wall temperature of 239 K so that the ratio of the wall enthalpy to the freestream enthalpy is 0.4. The coefficient of the normal force and pitching moments at various angles of attack are obtained on two grids, and the results are compared with the experimental values [18] in Figs. 3a and 3b, respectively. The computed coefficients on the finer grid compare well with the experimental results. The pressure distribution along the symmetry line on the windward and leeward surfaces at $\alpha = 0, 5, 10$, and 15 deg are compared with the experimental results and are given in Figs. 4a and 4b, respectively. The pressure on the windward side increases, whereas the leeward-side pressure decreases with an increase in angle of attack; and the pressure drops at the forebody and afterbody junction. There is a good agreement with the experimental results, but it is slightly underpredicted in the forebody pressure on the windward side at higher angles of attack. It can also be observed that the pressure is constant in the forebody, indicating conical flow; and it is decreasing in the afterbody due to a nonconical relieving effect. The surface heat transfer distributions along the centerline at $\alpha = 0$ and 15 deg are compared with the experimental results and are given in Figs. 5a and 5b, respectively. The Stanton number of $St = q/((\rho u)_\infty (H_t - H_w))$ is used for comparing the heat transfer rate q. Here, $(\rho u)_\infty$ is the freestream mass flow rate, H_t is the freestream total enthalpy, and H_w is the wall enthalpy. The windward surface heat transfer rates compare well with the experimental results at both angles of attack. At $\alpha = 15$ deg, there is a mismatch of heat flux in the windward side of the forebody, which may be due to flow transition. The grid-free code is able to predict aerodynamic forces and moments, pressure, and heat flux distributions accurately at very high Mach numbers and angles of attack. This case demonstrates the robustness of the grid-free code to capture strong shocks and high expansions, as well as accuracy in resolving boundary layer to predict heat fluxes.

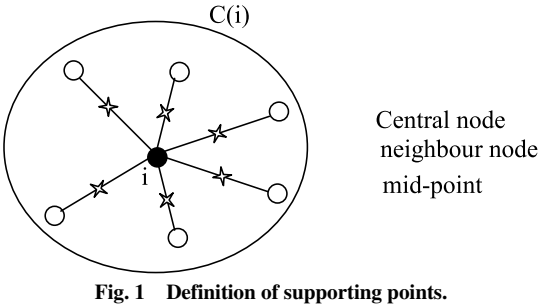

Fig. 1 Definition of supporting points.

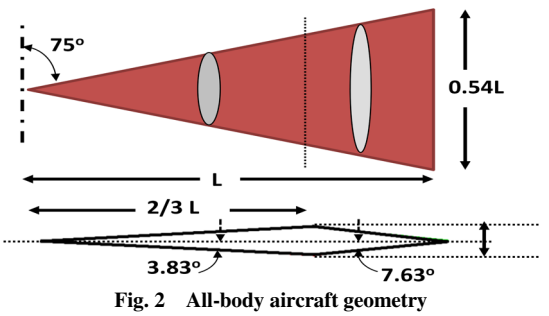

Fig. 2 All-body aircraft geometry

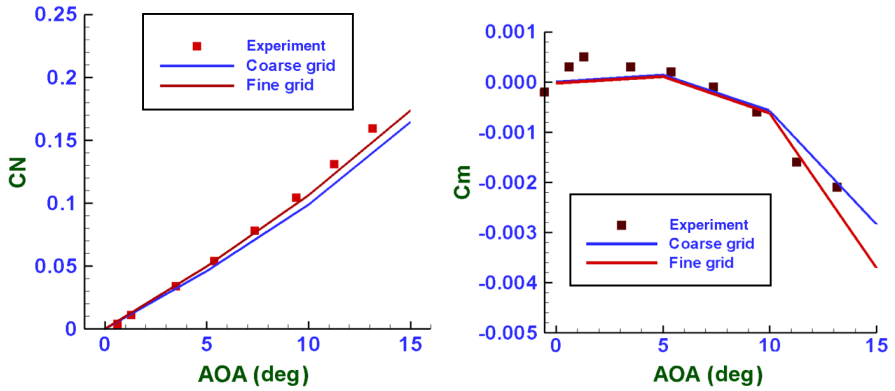

a) b)

Fig. 3 Comparison of aerodynamic coefficients with experiment at different angles of attack (AOA) on two grids: a) coefficient of normal force, and b) coefficient of pitching moment.

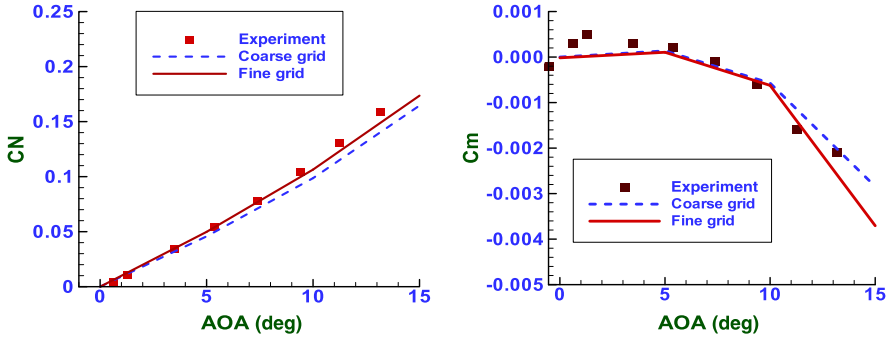

a) b)

Fig. 4 Comparison of surface pressure distributions at different angles of attack: a) windward side, and b) leeward side.

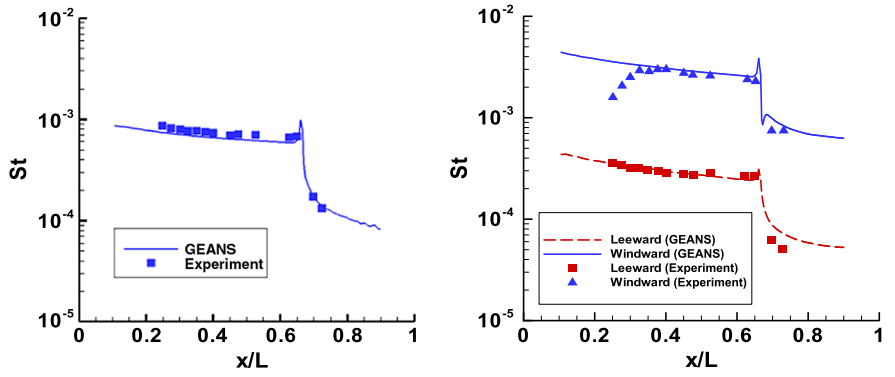

a) b)

Fig. 5 Comparison of axial distributions of heat flux at a) $\alpha = 0$ deg and b) $\alpha = 15$ deg.

IV. Conclusions

The 3-D implicit grid-free Reynolds averaged Navier–Stokes code GEANS has been developed. The one-equation Spalart–Allmaras turbulence model is used for turbulence closure. The code is validated for hypersonic all-body aircraft configuration. The point distributions are obtained using a structured grid generator. The hypersonic all-body aircraft is simulated at a Mach number of 7.4 and angles of attack up to 15 deg. Various flowfield and surface quantities, such as pressure and heat transfer rates, compare well with the experimental measurements; and the aerodynamic force and moment coefficients compare well with the experimental results. Considering the complex flowfields due to high Mach numbers and high angles of attack, the present prediction encourages the use of a grid-free solver for hypersonic viscous flows.

References

[1] Shaw, J. A., Stokes, S., and Lucking, M. A., "The Rapid and Robust Generation of Efficient Hybrid Grids for RANS Simulations Over Complete Aircraft," *International Journal for Numerical Methods in Fluids*, Vol. 43, Nos. 6–7, Oct.–Nov. 2003, pp. 785–821. doi:10.1002/(ISSN)1097-0363

[2] Chan, W. M., Pandya, S. A., and Rogers, S. E., "Efficient Creation of Overset Grid Hole Boundaries and Effects of Their Locations on Aerodynamic Loads," *21st AIAA Computational Fluid Dynamics Conference*, AIAA Paper 2013-3074, June 2013.

[3] Deshpande, S. M., Ghosh, A. K., and Mandal, J. C., "Least Square Weak Upwind Methods for Euler Equations," Indian Inst. of Science, Dept. of Aerospace Engineering, Rept. 89 FM4, Bangalore, India, 1989.

[4] Jahangirian, A., and Hashemi, M. Y., "Adaptive Cartesian Grid with Mesh-Less Zones for Compressible Flow Calculations," *Computers and*

Fluids, Vol. 54, No. 1, Jan. 2012, pp. 10–17.
doi:10.1016/j.compfluid.2011.08.010

[5] Deshpande, S. M., Anandhanarayanan, K., Praveen, C., and Ramesh, V., "Theory and Applications of 3-D LSKUM Based on Entropy Variables," *International Journal for Numerical Methods in Fluids*, Vol. 40, Nos. 1–2, Sept. 2002, pp. 47–62.
doi:10.1002/(ISSN)1097-0363

[6] Anandhanarayanan, K., Arora, K., Shah, V., Krishnamurthy, R., and Chakraborty, D., "Separation Dynamics of Air-to-Air Missile Using a Grid-Free Euler Solver," *Journal of Aircraft*, Vol. 50, No. 3, May–June 2013, pp. 725–731.
doi:10.2514/1.C031791

[7] Batina, J. T., "A Gridless Euler/Navier–Stokes Solution Algorithm for Complex-Aircraft Applications," *31st Aerospace Sciences Meeting & Exhibit*, AIAA Paper 1993-0333, Jan. 1993.

[8] Lohner, R., Sacco, C., Onate, E., and Idelsohn, S., "A Finite Point Method for Compressible Flow," *International Journal for Numerical Methods*, Vol. 53, No. 8, March 2002, pp. 1765–1779.
doi:10.1002/nme.334

[9] Su, X., Sasaki, D., and Nakahashi, K., "Cartesian Mesh with a Novel Hybrid WENO/Meshless Method for Turbulent Flow Calculations," *Computers and Fluids*, Vol. 84, No. 1, Sept. 2013, pp. 69–86.
doi:10.1016/j.compfluid.2013.05.017

[10] Kennett, D. J., Timme, S., Angulo, J., and Badcock, K. J., "An Implicit Meshless Method for Application in Computational Fluid Dynamics," *International Journal for Numerical Methods in Fluids*, Vol. 71, No. 8, March 2013, pp. 1007–1028.
doi:10.1002/fld.v71.8

[11] Katz, A., and Jameson, A., "Edge-Based Meshless Methods for Compressible Flow Simulations," *46th AIAA Aerospace Sciences Meeting and Exhibit*, AIAA Paper 2008-699, Jan. 2008.

[12] Chiu, E. K., Wang, Q., and Jameson, A., "A Conservative Meshless Scheme: General Order Formulation and Application to Euler Equations," *49th AIAA Aerospace Sciences Meeting including the New Horizons Forum and Aerospace Exposition*, AIAA Paper 2011-0651, Jan. 2011.

[13] Lockman, W. K., Lawrence, S., and Cleary, J. W., "Experimental and Computational Surface and Flow-Field Results for an All-Body Hypersonic Aircraft," AIAA Paper 1990-3067, 1990.

[14] Anandhanarayanan, K., "Development of a Grid-Free Viscous Solver," *Proceedings of 13th AeSI CFD Symposium*, CFD Division, Aeronautical Soc. of India, Paper CP-9, Bangalore, India, Aug. 2011, pp. 34–35.

[15] Spalart, P. R., and Allmaras, S. R., "A One-Equation Turbulence Model for Aerodynamic Flows," AIAA Paper 1992-0439, Jan. 1992.

[16] Kim, S.-S, Kim, C., Rho, O.-H., and Hong, S. K., "Cures for the Shock Instability, Development of a Shock-Stable Roe Scheme," *Journal of Computational Physics*, Vol. 185, No. 2, 2003, pp. 342–374.
doi:10.1016/S0021-9991(02)00037-2

[17] Barth, T. J., and Jespersen, D. C., "The Design and Application of Upwind Schemes on Unstructured Meshes," *27th Aerospace Sciences Meeting*, AIAA Paper 1989-0366, 1989.

[18] Nelms, W. P., Jr., and Thomas, C. L., "Aerodynamic Characteristics of an All-Body Hypersonic Aircraft Configuration at Mach Numbers from 0.65 to 10.6," NASA, Rept. TN-D-6577, Nov. 1971.

M. Smith
Associate Editor